Applied Catalysis B: Environmental 145 (2014) 126–135

Contents lists available at ScienceDirect

Applied Catalysis B: Environmental

journal homepage: www.elsevier.com/locate/apcatb

Highly productive iron molybdate mixed oxides and their relevant catalytic properties for direct synthesis of *1,1*-dimethoxymethane from methanol

Kaew-arpha Thavornprasert[a,b], Mickaël Capron[a,b,*], Louise Jalowiecki-Duhamel[a,b], Olivier Gardoll[a,b], Martine Trentesaux[a,b], Anne-Sophie Mamede[a,b], Ge Fang[a,b], Jérémy Faye[a,b], Nadia Touati[a,c], Hervé Vezin[a,c], Jean-Luc Dubois[d], Jean-Luc Couturier[f], Franck Dumeignil[a,b,e]

[a] *Univ. Lille Nord de France, F-59000 Lille, France*
[b] *CNRS UMR8181, Unité de Catalyse et Chimie du Solide, UCCS, F-59655 Villeneuve d'Ascq, France*
[c] *Laboratoire de Spectrochimie Infrarouge et Raman, Université Lille 1 Sciences et Technologies (CNRS UMR8516), F-59655 Villeneuve d'Ascq, France*
[d] *Arkema, 420 Rue d'Estienne d'Orves, 92705 Colombes, France*
[e] *Institut Universitaire de France, Maison des Universités, 103 Boulevard Saint-Michel, 75005 Paris, France*
[f] *Arkema France, CRRA, Rue Henri Moissan, 69493 Pierre Bénite, France*

ARTICLE INFO

Article history:
Received 19 November 2012
Received in revised form 22 January 2013
Accepted 23 January 2013
Available online 8 February 2013

Keywords:
Methanol oxidation
Acetalization
1,1-Dimethoxymethane, Iron molybdate catalysts

ABSTRACT

The one-step gas phase conversion of methanol to *1,1*-dimethoxymethane (DMM) was studied over highly productive iron molybdate mixed oxides in a fixed-bed reactor working at atmospheric pressure. When placing the Fe–Mo–O catalyst under a reaction mixture highly concentrated in methanol, the DMM selectivity was drastically boosted. This specific and unique feature encouraged us to extensively characterize this family of particular catalysts. LEIS analysis revealed the presence of both Mo and Fe species on the outermost atomic layer of the catalysts. X-ray photoelectron spectroscopy (XPS) and *in situ* EPR measurements showed that the Fe centres are responsible for the redox properties. The acidic properties of the FeMo mixed oxides were then attributed to anionic vacancies acting as Lewis acid sites produced by dehydroxylation of the catalyst surface. XPS analysis also showed that oxygen from the gas phase was responsible for reoxidation of the catalyst surface with regeneration of the active sites, which suggests a Mars–van Krevelen mechanism. The good catalytic performances were then attributed to a synergistic effect between Mo and Fe species. A Mo/Fe molar ratio of 3.2 for an optimal remarkable yield in DMM of 50% was found.

1. Introduction

The disastrous environmental issues caused by the extensive consumption of fossil-based sources, especially for energetic needs, has driven numerous studies to find alternative sustainable resources. In this context, it is now well understood that biomass, which is an abundant and renewable feedstock, has a great potential for being used as a raw material for a large spectrum of high value-added chemicals, including fuel applications. Among the various envisioned target molecules, *1,1*-dimethoxymethane is of topical interest. It can be synthesized from the so-called 'bio-methanol' obtained *via* biomass-derived syngas conversion, which is an elegant way of cascade upgrading, and does not rely only on bio-based sourcing. DMM is distinguished by its versatility for various applications. It is widely used as a solvent and a starting material in the fragrance and pharmaceutical industries [1]. It is applied as a starting monomer in the synthesis of polyoxymethylene dimethylether (POMM), which could be used as a safe embalming agent in substitution of the currently used formaldehyde [2], a well-known human carcinogen. It finds also an application as an oxygenated additive to diesel fuel, particularly helping in the reduction of particles emissions, of which the great harm to human health has been recently widely covered by the media [3,4]. At last, DMM and POMM are also considered as alternative fuels for low-temperature fuel cells, much safer than methanol, due to, *e.g.*, for POMMs lower volatility [5–8]. It appears then that DMM has a lot of advantages from the environmental point of view, which explains the recently renewed interest concerning this molecule.

* Corresponding author at: Univ. Lille Nord de France, F-59000 Lille; CNRS UMR8181, Unité de Catalyse et Chimie du Solide, UCCS, F-59655 Villeneuve d'Ascq, France. Tel.: +33 3 20 43 69 85.
E-mail address: Mickael.Capron@univ-lille1.fr (M. Capron).

0926-3373/$ – see front matter © 2013 Elsevier B.V. All rights reserved.
http://dx.doi.org/10.1016/j.apcatb.2013.01.043

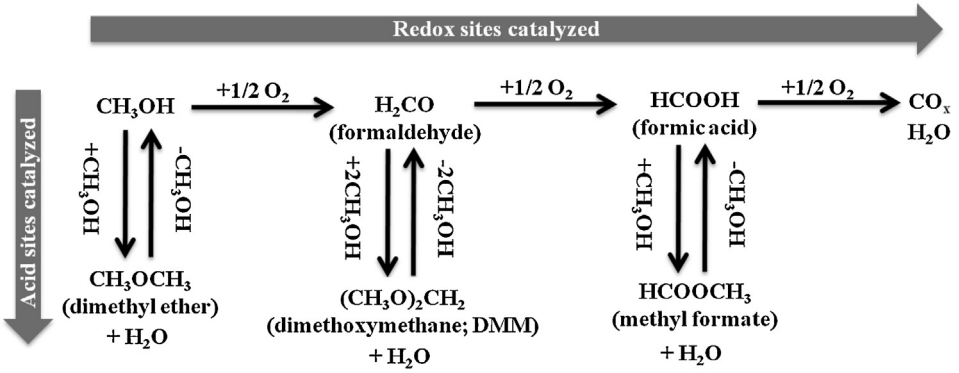

Scheme 1. Methanol oxidation pathways [29].

Production of DMM at the industrial scale is being currently carried out in a sequential way *via* two consecutive steps: gas phase methanol partial oxidation to formaldehyde, which is followed, in a second dedicated reactor, by liquid phase acetalization of the so-obtained formaldehyde with methanol molecules, including using reactive distillation process [9,10]. Synthesizing DMM *via* a single step direct route starting from methanol would obviously be preferred, thus minimizing the Capital Expenditure (CAPEX) and the production cost but also energy consumption besides reducing the environmental impact generated along the two-steps process. In this respect, developing selective catalysts for the one step partial oxidation of methanol to DMM is challenging, and has become a relatively widespread research subject in the recent years [11–28]. It has been reported that the direct reaction is strongly sensitive to the nature of the catalytic active sites [29]. Indeed, as shown in Scheme 1, the redox-catalyzed pathway leads to a sequence of oxidized species, namely formaldehyde, formic acid and carbon oxides, whereas the acid-catalyzed pathway yields dehydration products, *i.e.*, dimethyl ether, DMM and methylformate, respectively obtained from condensation of methanol with its aforementioned oxidation products. An appropriate system for the direct synthesis of DMM must thus be a bifunctional catalyst with adequate balance between redox and acid sites of the proper respective strength, in order to guide the reaction through the desired pathway among the possible ones in Scheme 1.

Various studies aiming at realizing the one-step methanol oxidation to DMM over a variety of catalytic systems, *i.e.*, molybdenum-based catalysts [11], heteropolyacids (HPAs) [12], oxides of ruthenium [13] and of rhenium [15–18], as well as vanadium-based catalysts [19–27] can be found in the literature. In the studies reporting the use of bulk and supported 12-molybdophosphoric acid catalysts, up to 55% of DMM selectivity was obtained at low methanol conversion of less than 20% [11]. Liu et al. investigated the performances of supported $H_{3+n}V_nMo_{12-n}PO_{40}$ polyoxometallate Keggin clusters. They reported a selectivity to DMM of 58% at a methanol conversion of 68% over 9.2 wt.% supported $H_4PVMo_{11}O_{40}/SiO_2$ [12]. These authors further examined the performances of a completely different system, namely RuO_2 supported on TiO_2, Al_2O_3 and TiO_2–Al_2O_3. They reported a maximum DMM selectivity of 67% at a lower conversion of 20% over a 4.4 wt.% Ru/Al_2O_3 catalyst [13]. Iwasawa and co-workers focused their investigations on ReO_x and Re-based mixed oxides supported on various solids, *i.e.*, TiO_2, SiO_2, V_2O_5, ZrO_2, α-Al_2O_3, α-Fe_2O_3, and γ-Fe_2O_3. Among the tested catalysts, Re/γ-Fe_2O_3 was the most efficient one with 91% selectivity to DMM at 48% conversion of methanol [15]. Following the results of Iwasawa's group, Sécordel et al. concentrated their study on supported TiO_2-anatase and SiO_2 oxorhenate catalysts prepared by thermal spreading of metal Re^0. A maximum DMM selectivity of 77% at 44% methanol conversion was claimed over a Re/TiO_2 catalyst [17]. Additionally, an attempt to use vanadium-containing catalysts has been described by several groups. Fu et al. reported a maximum DMM selectivity of 92% at 48% methanol conversion over the acid-modified V_2O_5/TiO_2–$Ti(SO_4)_2$ catalyst [19]. Later on, Lu et al. studied the V_2O_5/TiO_2 system [21–23] and further improved its catalytic reactivity by addition of SO_4^{2-}. 93% selectivity to DMM at 49% methanol conversion was reported over the catalyst loaded with 15 wt.% V_2O_5 and 15 wt.% SO_4^{2-} [24]. The performances of supported VO_x/TS-1 zeolite doping with SO_4^{2-} and PO_4^{3-} ions were then determined by Chen et al. Despite the fact of using a reactant feed within the flammable region – *i.e.*, methanol/O_2/N_2 = 1/2.5/7.5 (v/v), the authors reported a positive effect when adding SO_4^{2-} into VO_x/TS-1 catalyst that the so-obtained methanol conversion was significantly higher (46% compared with 24% for the unmodified catalyst) with essentially the same selectivity (81% *vs.* 83%) [25]. Guo et al. reported 90% of selectivity to DMM at 17% conversion of methanol over the V_2O_5/CeO_2 catalyst loaded with 15 wt.% V_2O_5 [26]. Developments of Sb-, V-, and Nb-containing catalysts for the oxidation of methanol were also discussed by Golinska-Mazwa et al. It was found that, by using a proper synthesis procedure for $SbVO_x$ mixed oxides further modified with Nb species, it was possible to obtain selective catalysts for DMM production [27]. A maximum yield in DMM was stated at 39% conversion of methanol with 36% DMM selectivity.

In this study, we used an iron molybdate mixed oxides catalyst [$Fe_2(MoO_4)_3$–MoO_3] [30], which is being currently used in the industry for formaldehyde production using reactant feeds with low methanol concentrations of less than 7.5 mol.% [22,23,31,32]. We optimized this catalytic system for DMM production, based on the hint that in our experiments DMM was always detected as a by-product, indicating the presence of an acid function that should be tuned to focus the selectivity. Then, in a previous study, we evaluated the performance of iron molybdate catalyst towards DMM formation in comparison with those of two very efficient catalysts used as benchmarks, namely Re/TiO_2 and an amorphous mixed oxide of Mo, V, W, Cu, and Sb [28,33]. It was demonstrated that the selectivity to DMM could be drastically increased by simply placing the iron molybdate catalyst under a reaction feed highly concentrated in methanol (40 mol.% of CH_3OH in air) while keeping the same methanol conversion as that observed in a methanol-poor feed (7.5 mol.% of CH_3OH in air). A remarkably high productivity of 4.6 $kg_{DMM}\ h^{-1}\ kg_{cat}^{-1}$, the highest value ever reported in the literature, was achieved with 56% of methanol conversion and 96% of DMM selectivity at 553 K. This performance boost observed upon shifting from methanol-poor to methanol-rich feed was not observed over the supported Re and the amorphous mixed oxide catalysts. Thus, the present work aims at investigating the redox and acid properties of the iron molybdate catalytic system to

correlate these properties to the catalytic behaviour in the direct synthesis of DMM from methanol, as the excellent performances of this system could hardly be explained without using advanced characterization methods, as those proposed in the present work. Better understanding of this system could indeed give precious hints for further developments towards industrialization.

2. Experimental

2.1. Catalysts preparation

Iron molybdate catalysts with Mo/Fe ratios between 2.5 and 4 were prepared by coprecipitation of the appropriate amount of aqueous solutions of $(NH_4)_6Mo_7O_{24}{\cdot}4H_2O$ (AHM; Fluka, 99%) and $FeCl_3{\cdot}6H_2O$ (Sigma-Aldrich, 98%), according to a procedure described by Pernicone et al. [34,35]. The AHM solution (pH ~ 5) was first acidified with HCl to reach a pH close to 1. The iron chloride solution was then continuously poured to the AHM solution under vigorous stirring at a temperature kept between 323 and 333 K. The obtained yellowish precipitate was maintained under agitation for 1 h in its mother liquor. After subsequent decantation of this solution during several hours, the chloride content of the top solution, which was then to be discarded, was evaluated. The precipitate was washed with water before performing again a decantation step, and this operation was repeated until chloride concentration was less than 2000 ppm. The presence of excess chloride ions was a crucial parameter, as it would, *e.g.*, decrease the acidity of the resulting catalyst. For checking that the catalysts were sufficiently Cl-free, we used the following procedure. A reference solution of 2000 ppm of Cl^- was prepared by dissolving 3.297 g of NaCl in 1 L of distilled water. 5 mL of the discarded solution and 5 mL of the reference solution were placed in different volumetric flasks of 25 mL. 2 mL of calibrated $AgNO_3$ acidified by nitric acid was added in each flask. The intensity of the white $AgCl_{(s)}$ precipitate obtained from the discarded solution was compared to that of the reference to assess whether further purification sequence was needed. When the Cl^- concentration was then lowered to the desired extent, the precipitate was filtered and dried at 383 K for 4 h. The recovered solid was crushed in a mortar before being pelletized using an IR press. The obtained pellets were further sieved to gather particles with a diameter comprised between 2 and 3 mm. These particles were subsequently calcined in air (0.3 L min^{-1}) at 723 K for 2 h. The calcined catalysts were subsequently sieved to particles of 250–500 μm diameters before evaluation of their catalytic performances. The catalysts were arbitrarily named in numerical order as FM01, FM02, FM03, FM04 and FM05 (*cf.* Section 3.1, Table 1).

Single oxides Fe_2O_3 and MoO_3 samples were additionally prepared as references for Mo-free and Fe-free catalysts, respectively. Commercial Fe_2O_3 (Merck, 99%) was calcined at 623 K in air for 2 h. The Mo precursor, AHM, was calcined at 723 K for 6 h in air. The calcined powders were similarly sieved to particles of 250–500 μm diameters before measuring their catalytic performances.

2.2. Characterization techniques

X-ray diffraction (XRD) spectra of the calcined catalysts were obtained on a D8 Advance apparatus (Bruker AXS). The diffraction pattern was recorded between 10° and 60° (2θ) with 0.02° steps (integration time 1.5 s). Elemental analysis was carried out by inductively coupled plasma-mass spectroscopy (ICP-MS) using a Thermo-Fischer X7 ICP-MS device. The specific surface areas of the calcined catalysts were determined using the single-point BET (Brunauer, Emmett, Teller) method, with N_2 adsorption at liquid N_2 temperature and subsequent desorption at room temperature. The samples were outgassed at 473 K for 30 min prior to analysis.

Elemental identification of the atoms located on the outer surface of the samples (top atomic layer) was determined by low-energy ion scattering (LEIS). The spectra were recorded on a Qtac^{100} spectrometer (ION TOF GmbH) described elsewhere [36]. The LEIS spectra were obtained using 3 keV $^4He^+$ scattering. Assuming a sputter yield of 0.1 atoms per He-ion under a 4 nA target current, only 3.0×10^{13} cm^{-2} atoms were sputtered from the sample surface during the analysis. The catalysts surface was further investigated by X-ray photoelectron spectroscopy. The analyses were performed with a VG ESCALAB 220XL spectrometer (Thermo) using the AlKα radiation (1486.6 eV) in the large area lens mode. The surface composition was then obtained from measurement of the Mo 3d, Fe 2p, C 1s, and O 1s levels, obtained at a 40 eV pass energy. The C 1s binding energy for the C—(C,H) bond was fixed at 285 eV as an internal reference. The measurements were carried out under vacuum (around 10^{-7} Pa). The simulation of the experimental photopeaks was carried out using the CasaXPS software [37]. The non-pre-treated catalyst was first analyzed under its freshly prepared form by XPS before being analyzed again after pre-reduction in a dedicated treatment chamber placed under methanol-rich helium atmosphere (20 mol.% methanol) at 528 K, without intermediate re-exposure to the air. A second measurement was then performed after pre-treatment in oxygen and methanol flow in He (CH_3OH/O_2/He = 20/16/64 mol.%, for simulating air condition) in order to perform partial oxidation reaction. *In situ* electron paramagnetic resonance (EPR) spectra were collected with an X-Band Bruker ELEXYS E580 spectrometer operating at a 100 kHz modulation frequency and a 2 G modulation amplitude. The microwave power was set to 1 mW. The special cell used for this study is described elsewhere [38]. The fresh catalyst was firstly placed in a cell inserted in a dual cavity at room temperature under vacuum. The treatment temperature was gradually increased to 528 K. Afterwards a reactant mixture (CH_3OH/O_2/He = 20/16/64 mol.%) was introduced in the analysis chamber.

The acidity of the fresh catalysts was evaluated by NH_3-TPD using a Micromeritics Autochem 2920 apparatus coupled with a mass spectrometer Omnistar. The freshly prepared catalyst were outgassed under a helium flow of 40 mL min^{-1}, while being heated from room temperature to 523 K with a heating rate of 10 K min^{-1}, the final temperature being kept 30 min to ensure total elimination of physisorbed water molecules, before cooling to room temperature under He. Adsorption of NH_3 was then performed at room temperature using a 30 mL min^{-1} flow of 10% of NH_3 in helium for 30 min before the sample was purged with pure helium (50 mL min^{-1}) for 2 hours to remove physisorbed NH_3. Desorption of NH_3 was then performed applying a heating rate of 10 K min^{-1} from room temperature to 873 K under a He flow of 10 mL min^{-1}, this final temperature being further kept during 1 h. In another set of experiments, the samples were also partially reduced with pure H_2 (40 mL min^{-1}) at 553 K for 1 h before being subjected to TPD experiments, in order to check the acidic properties of reduced catalysts. The recorded NH_3 signals were fitted using the DMFit software [39].

2.3. Activity measurements

The methanol partial oxidation reaction was carried out in a fixed-bed reactor at different temperatures between 503 and 563 K under atmospheric pressure. A schematic diagram of the setup is described elsewhere [31]. The reactor was loaded with 150 mg of catalyst diluted with the same amount of carborundum (250 μm). The reaction feed was carefully chosen outside the explosive zone of the mixture. It consisted of 40/13/47 mol.% of CH_3OH/O_2/He in order to simulate a methanol/air ratio. The gas hourly space velocity (GHSV) was adjusted to 16 NL h^{-1} $g_{cat}{}^{-1}$. The reaction products were analyzed every 20 min until stabilization

Table 1
Physical properties of the calcined catalysts prepared with different Mo/Fe nominal atomic ratios.

Catalyst	S_{BET} ($m^2\ g^{-1}$)	Mo/Fe ratio			Fe/M_T [a]	Amount of crystalline phase (rel.%)	
		Theoretical	ICP-MS	LEIS		$Fe_2(MoO_4)_3$	MoO_3
FM01	2	2.5	2.5	4.0	0.283	87	13
FM02	7	3	2.8	2.4	0.260	77	23
FM03	11	3.5	3.5	4.1	0.222	80	20
FM04	10	3.75	3.4	2.7	0.228	64	36
FM05	5	4	3.9	3.0	0.205	52	48
Fe_2O_3	2	–	–	–	1	–	–
MoO_3	4	–	–	–	0	–	100

[a] From ICP-MS measurements.

(measurements at the steady state) using an online gas micro chromatograph (SRA3000) equipped with two columns (plot U and molecular sieves) and two thermal conductivity detectors. In any experiment, the carbon balance was comprised between 95 and 105%, which underlines accuracy of the measurements.

3. Results and discussion

3.1. Preliminary characterizations – catalyst composition, textural property and X-ray diffraction

It has been reported that the iron molybdate mixed oxide catalysts consist of two or three crystalline phases depending on the synthesis parameters [28,31,33]. The XRD patterns of the prepared catalysts exhibit characteristic peaks of ferric molybdate and molybdite phases, as shown in Fig. 1. The respective amount of each main phase present in the catalysts was determined from their diffractograms using the Eva software (Table 1). It is notable that the relative amount of MoO_3 phase present in the catalyst reasonably increases with the Mo/Fe atomic ratio. Nonetheless, no significant correlation could be observed between the specific surface area – which remained low in any case, less than or equal to 11 $m^2\ g^{-1}$ – and the Mo/Fe ratio. The ICP-MS atomic composition of the samples are also given in terms of Mo/Fe atomic ratios, with values of 2.5, 2.8, 3.5, 3.4 and 3.9, respectively – corresponding to Fe/M_T values, where M_T = Fe + Mo, of 0.283, 0.260, 0.222, 0.228 and 0.205. These values obtained from ICP-MS technique are quite different from those obtained by LEIS, meaning that it exists a non-homogeneous distribution of the different atoms (*i.e.*, Mo and Fe) within the matrix between the bulk and the surface of the catalysts.

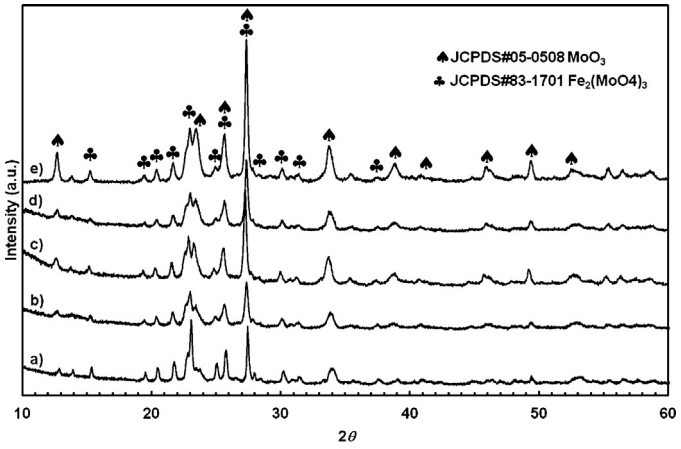

Fig. 1. X-ray diffractograms of the calcined samples: FM01 (a), FM02 (b), FM03 (c), FM04 (d) and FM05 (e).

3.2. Catalytic performance tests

Fig. 2 presents the catalytic performances of the mixed oxides samples at 528 K, which was the optimal temperature for DMM production. During the reaction, a methanol conversion gradually increased with time on stream before stabilizing. FM04 exhibited the highest conversion of 46%. FM02 and FM03 showed similar methanol conversions (*ca.* 35%), whereas FM05 gave a 19% conversion. The lowest conversion was however observed over FM01 (17%), possibly due to its particularly low specific surface area (2 $m^2\ g^{-1}$). Irrespective of the sample, the same trend was observed concerning DMM selectivity evolution, which gradually increased with time on stream before stabilizing after 4–5 h. The highest DMM selectivity was observed over FM01 (93%), certainly linked with the low conversion of this sample (*i.e.*, at low methanol conversion the quantity of methanol that can react with oxidized intermediates (formaldehyde, methoxy group, *etc.*) is high leading to this high selectivity in DMM). Likewise, a high selectivity to DMM of 89% was obtained with FM05, which also exhibited a rather low conversion (19%). A considerably high DMM selectivity of 85% was however still observed over FM02, FM03 and FM04. As a consequence of its high conversion, FM04 with a Mo/Fe bulk atomic ratio of 3.4 exhibited the highest yield in DMM. This sample is also the one that exhibited a relatively large amount of MoO_3 phase (36%) together with a relatively high specific surface area (10 $m^2\ g^{-1}$) in comparison to the other samples.

The catalytic performance indicators (methanol conversion, DMM selectivity and DMM yield) can be reported relative to the Fe proportion in the samples. In Fig. 3, these parameters are plotted *vs.* Fe/M_T. Clearly, an optimal DMM yield of 50% might be extrapolated for a Fe/M_T ratio of about 0.24 (Mo/Fe = 3.2) (Fig. 3B). The performances of the Fe_2O_3 and the MoO_3 samples, thus with Fe/M_T = 1 and 0, respectively, have also been checked. A stable conversion of 7% is obtained over Fe_2O_3 without any DMM formation. This sample is selective to methyl formate (80%) and formaldehyde (20%), which suggests the presence of exclusively redox properties. On the other hand, MoO_3 exhibited a high selectivity to DMM of 80% at the same methanol conversion of 7%. This suggests that MoO_3 has the intrinsic properties to yield DMM (*i.e.*, redox and acidic properties), which are then boosted in the presence of Fe in the mixed oxide, with a synergetic effect on conversion. Fig. 3B shows a close-up of Fig. 3A for Fe/M_T ratios between 0.2 and 0.3. This figure evidences that high DMM yields are obtained in a very narrow range of Fe contents, *i.e.*, 30–40% yields in DMM are achieved with the Fe/M_T ratios between 0.22 and 0.26).

3.3. Intensive characterizations

3.3.1. Low-energy ion scattering

Evolution of the catalyst surface has been investigated by LEIS and XPS. The LEIS spectra recorded in static conditions (*i.e.*, less than 1% of a monolayer was sputtered during one spectrum), of iron

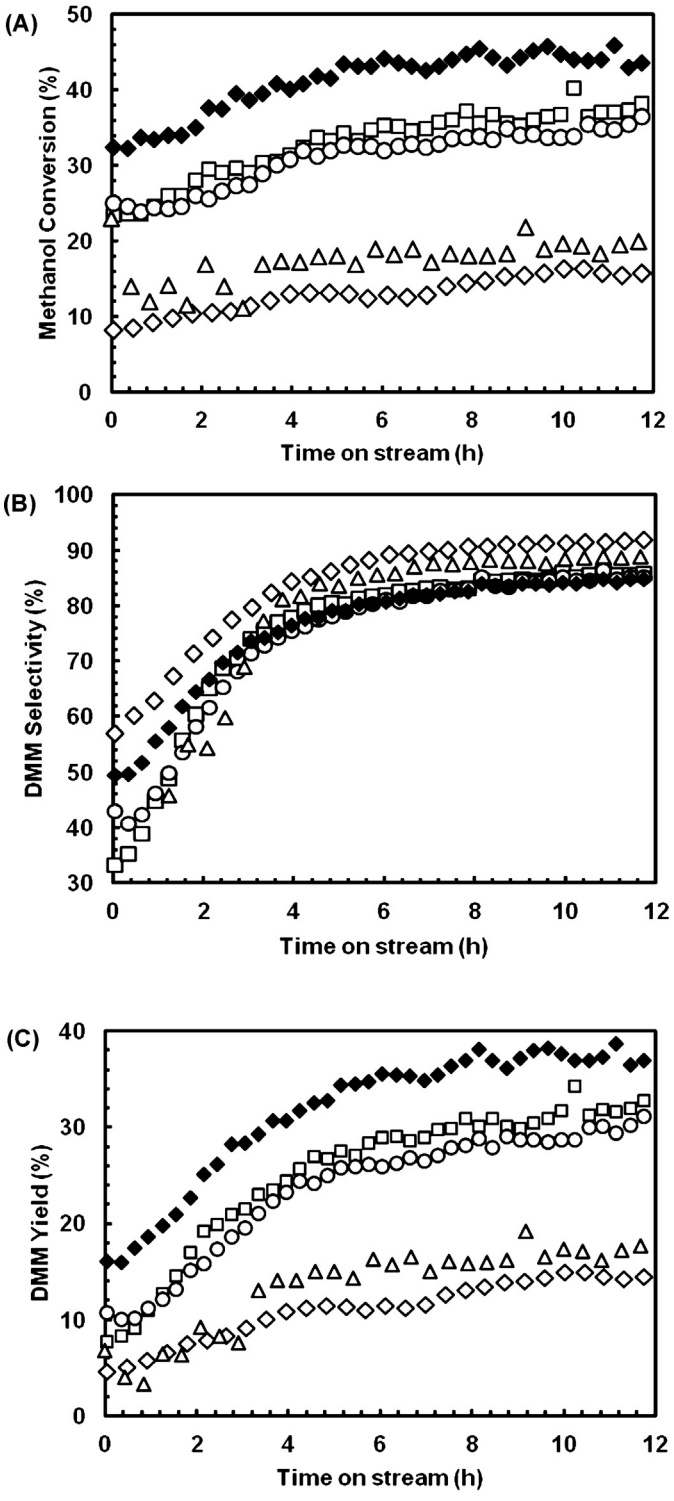

Fig. 2. Evolution with time on stream of methanol conversion (A), DMM selectivity (B), and DMM yield (C) observed over FM01 (◊), FM02 (□), FM03 (○), FM04 (♦) and FM05 (△) catalysts. Experimental conditions: GHSV = 16 NL min^{-1} g^{-1}, T = 528 K, $CH_3OH/O_2/He$ = 40/13/47 mol.%.

molybdate mixed-oxides with different Mo/Fe ratios are presented in Fig. 4A. They reveal that both Mo and Fe species are exposed at the outermost atomic layer of the catalysts. In particular, the catalyst giving the highest DMM yield (FM04) presents a surface Mo/Fe ratio of 2.7. This value is slightly lower than the bulk one determined by ICP-MS, *i.e.*, Mo/Fe = 3.4. LEIS sputtering series have been recorded on this catalyst to determine the evolution of relative

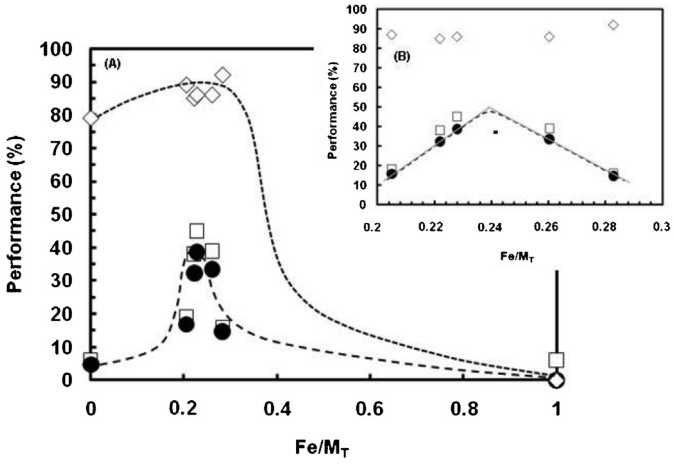

Fig. 3. (A) Performance after 12 h on stream as a function of the Fe/M_T molar ratio (with Fe + Mo = M_T); methanol conversion (□), DMM selectivity (◊), and DMM yield (●); (B) zoom-in results for Fe/M_T ratios between 0.2 and 0.3.

quantities of Mo and Fe species present at the outermost surface layer. The evolution of the relative intensities of Mo, Fe and O peaks with the He^+ ion fluence from 3 keV $^4He^+$ LEIS spectra of the FM04 catalyst is depicted in Fig. 4B. Along the sputtering experiments, the intensity of Mo peak was significantly higher than those of Fe and O peaks, suggesting that surface contaminants preferentially interacted with Mo species on the surface. Development of Mo/Fe ratio from $^4He^+$ LEIS spectra of the FM04 catalyst with the He^+ ion fluence is presented in Fig. 4C. At the beginning of the experiments, the outer monolayer exhibited a Mo/Fe ratio of 2.4. The Mo concentration increased with progressive exposure of the second atomic layer till a Mo/Fe ratio of around 4. Assuming a surface layer of 10^{15} atoms cm^{-2}, an estimated depth of around 0.7 monolayer has been eroded after the successive LEIS analyses – in other words, 30% of the outer layer remained after these sputtering experiments and 70% of the underneath layer was consecutively revealed. An average Mo/Fe ratio of 3.6 can then be estimated, taking into account the values of Mo/Fe determined at the beginning (Mo/Fe = 0.3 × 2.4) and at the end (Mo/Fe = 0.7 × 4) of the successive experiments. This so-obtained averaged Mo/Fe ratio is thus in a good agreement with that determined from elemental analysis (Mo/Fe = 3.4) – the bulk ratio that would probably be revealed in case of the complete erosion of the outermost surface layer.

3.3.2. X-ray photoelectron spectroscopy

Surface composition and oxidation state were inferred from XPS measurements. FM02 was chosen as a representative of the catalysts in the studied series. This catalyst was considerably reactive with significant conversion and selectivity (35% and 85%, respectively). It also presented relatively high amount of $Fe_2(MoO_4)_3$ phase (77%), which was useful to reliably observe any change occurring on Mo and Fe centres. Fig. 5 presents an evolution of the XPS Fe 2p spectra of FM02 after different treatment conditions. The shape and positions of the Fe 2p photopeaks assigned to Fe atoms in the fresh catalyst (Fig. 3A) corresponds only to Fe^{III} species [40]. Indeed, the Fe $2p_{3/2}$ peak located at 711.2 eV presents a characteristic asymmetry due to multiplet splitting of high spin Fe^{III} ions [41] and it has an associated satellite peak located at around 8 eV at higher energy. After exposure to the CH_3OH/He mixture for 60 min, a new set of components appears at lower BEs on the Fe 2p signal (Fig. 5B). They are attributed to the formation of Fe^{II} species. Indeed, the BE for Fe $2p_{3/2}$ is 709.0 eV associated with a satellite peak at around 6 eV higher energies. Thus, Fe^{III} centres are partially reduced under the flow of CH_3OH-He before reaching a surface composition of 46% of Fe^{II} and 54% of Fe^{III} at the end of the treatment (Table 2).

Table 2
XPS analysis results after one hour on stream with FM02 sample after different *in situ* treatments at 528 K in 20 mol.% of methanol in air.

Treatment condition	Binding energy (eV)		Peak width (FWHM)		Relative atomic conc. of Fe $2p_{3/2}$ species (%)		Mo/Fe XPS atomic ratio
	Mo $3d_{5/2}$ (Mo^{VI})	Fe $2p_{3/2}$ (Fe^{III})	Mo $3d_{5/2}$ (Mo^{VI})	Fe $2p_{3/2}$ (Fe^{III})	Fe^{III}	Fe^{II}	
Fresh catalyst	232.3	711.2	1.9	4.3	100	–	3.0
Air (O_2/He)	232.0	712.2	1.6	4.8	100	–	5.1
CH_3OH/He	231.6	709.0	2.4	4.3	54	46	4.8
CH_3OH/O_2/He	232.6	712.2	1.6	3.9	71	29	3.4

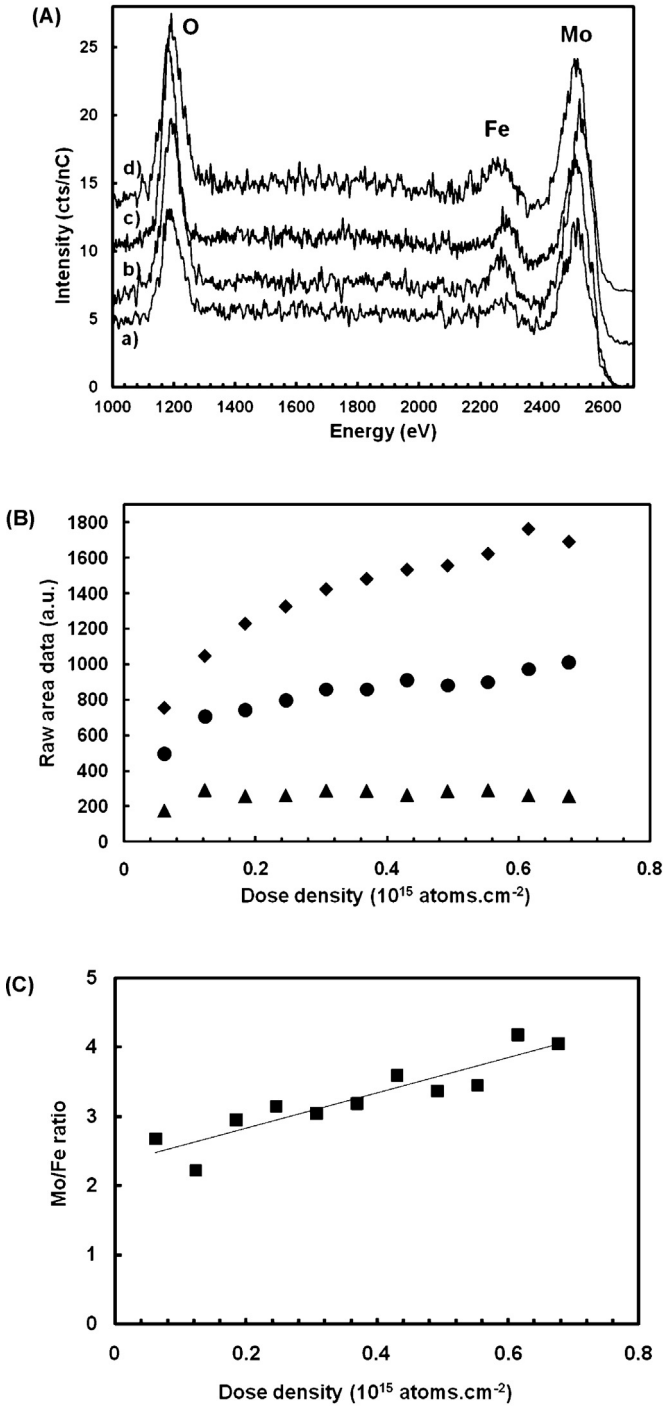

Fig. 4. (A) 3 keV $^4He^+$ LEIS spectra of iron molybdates: FM01 (a), FM02 (b), FM03 (c), and FM04 (d); (B) evolution of relative intensities of Mo (♦), Fe (▲) and O (●) peaks with the He^+ ion fluence from 3 keV $^4He^+$ LEIS spectra of FM04 catalyst during sputtering experiments; (C) evolution of the Mo/Fe ratio from 3 keV $^4He^+$ LEIS spectra of FM04 catalyst with the He^+ ion fluence.

When oxygen is further added to the pre-treatment gas mixture, the proportion of Fe^{II} decreased to 29% (Fig. 5C). This evidences the partial re-oxidation of Fe^{II} by molecular oxygen on the surface or by the Mars–van Krevelen mechanism (O migration). On the contrary, no significant change in BE values for Mo centres was evidenced. A Mo 3d doublet located at 232.3 and 236.3 eV is present, corresponding to the characteristic BE values of Mo $3d_{5/2}$ and Mo $3d_{3/2}$ for Mo^{VI} species, respectively [42]. However, a slight shift of 0.4 eV is observed for both peaks when the catalyst has been exposed to the mixture of CH_3OH–He. This shift to lower BE (231.6 eV) for Mo $3d_{5/2}$ cannot be explained by a partial reduction of Mo^{VI} as the BE values of Mo 3d for Mo^V species are reported in literature with a

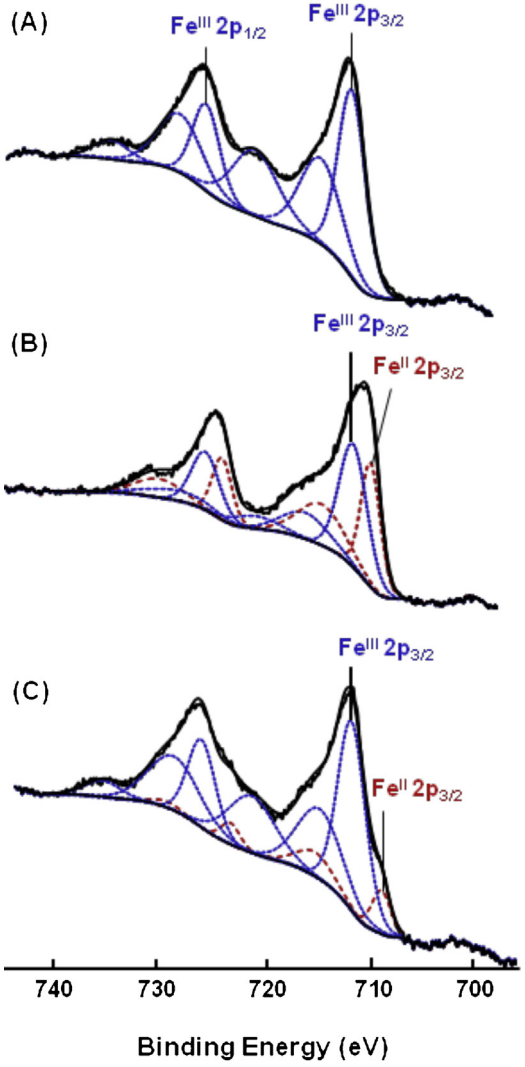

Fig. 5. XPS analyses of the Fe 2p level for the FM02 sample under different conditions: fresh catalyst (A), CH_3OH/He after 60 min (B), and CH_3OH/O_2/He after 60 min (C).

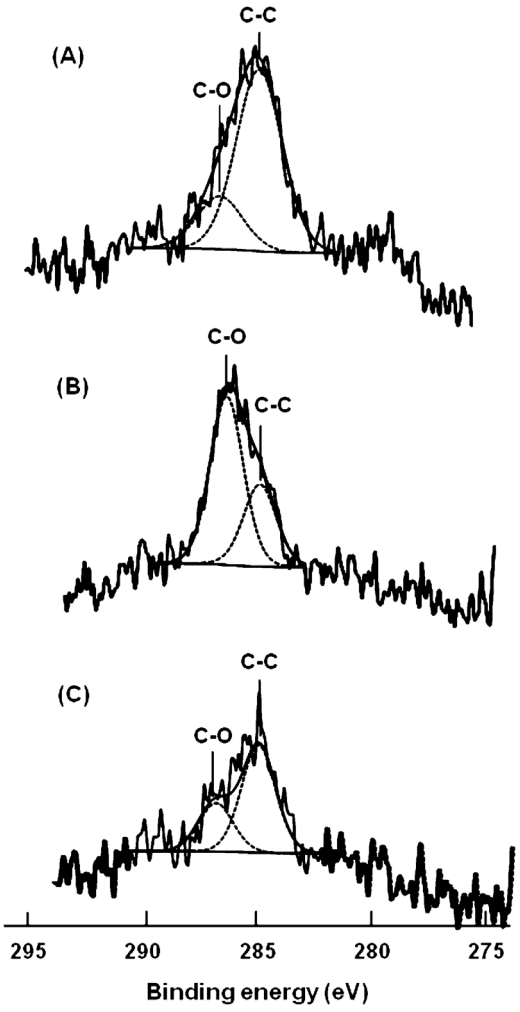

Fig. 6. XPS analyses of the C 1s level for the FM02 sample under different conditions: fresh catalyst (A), CH_3OH/He after 60 min (B), and CH_3OH/O_2/He after 60 min (C).

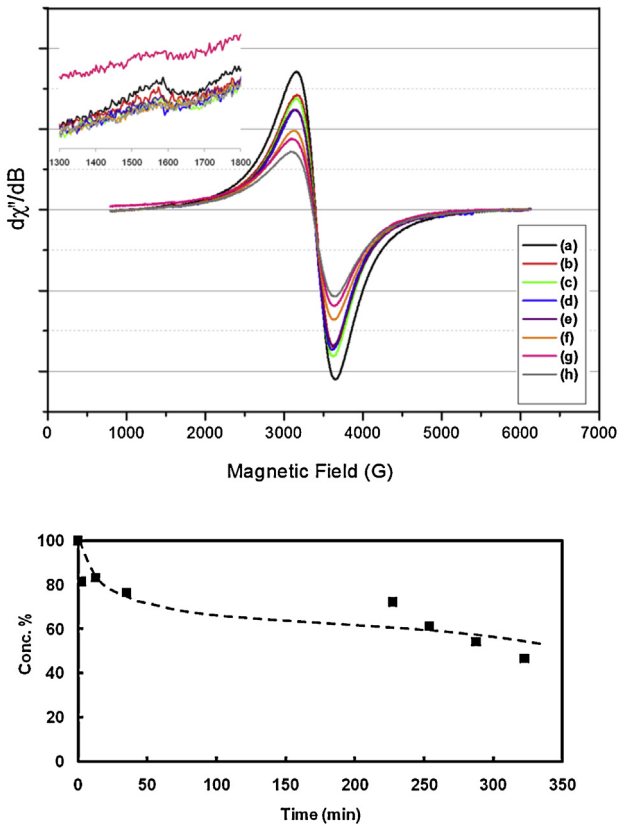

Fig. 7. (A) Evolution of EPR Fe^{III} signal at $g = 2.002$ with a magnification of the signal at $g = 4.17$ recorded for the fresh FM04 powder at room temperature (a), powder at 528 K with no gas flow (b), powder treated under 20 mol.% $CH_3OH/Ar/O_2$ flow at 528 K at $t = 0$ (c), after 25 min (d), 215 min (e), 240 min (f), 275 min (g), and 320 min (h); (B) evolution of the quantity of Fe^{III} as determined by EPR spectroscopy deduced from (A).

difference of 1.6 eV from those of Mo^{VI} [43]. Moreover, an increase in the peak width (FWHM) of Mo $3d_{5/2}$ peak (0.8 eV) is observed, associated with a slight shift to lower BE of this peak, when placing the catalyst under the reducing atmosphere (CH_3OH–He). Based on this observation, while the oxidation degree of Mo (in iron molybdate) remains VI, its environment is disturbed and, therefore, it is not in a fully oxidized state.

At the same time, we observed in the C 1s energy domain, a significant increase in the contribution of the C—O component located at 286.5 eV (Fig. 6B), which is attributed to the formation of methoxy groups (CH_3O—) [44], due to the dissociative adsorption of methanol at the surface of the catalyst. Also, note that the fresh catalyst already showed the characteristic feature of surface contamination by carbon (Fig. 6A). The combined changes observed on Mo and C suggest that the methoxy groups are presumably linked with Mo atoms. The position of the Mo $3d_{5/2}$ photopeak shift back to its initial value (232.6 eV) when the oxygen flow is introduced into the feed mixture evidences desorption of methoxy groups from the surface and/or their surface reaction.

The surface atomic composition changed according to the different treatment conditions (Table 2), especially after treating the catalyst under air and CH_3OH/He conditions, where Mo enrichment on the surface is observed, with atomic Mo/Fe ratios of 5.1 and 4.8, respectively. When considering the catalyst placed in the flow of CH_3OH/O_2/He, the Mo/Fe ratio variation is not so significant even if a partial reduction of the solid occurs as evidenced by the presence of Fe^{II}. The Mo/Fe ratio of 3.4 is determined after the treatment in the presence of the reactants mixture. The so-obtained value is close to that of the fresh catalyst (Mo/Fe = 3.0). It is notable that, for the fresh catalyst, the atomic Mo/Fe ratio at the surface measured by XPS is in a good agreement with that determined by ICP-MS (Mo/Fe = 2.8; *cf.* Section 3.1, Table 1), meaning that the bulk and the surface have essentially the same composition.

3.3.3. Electron paramagnetic resonance

In situ EPR experiments were carried out at 528 K with the best catalyst, namely FM04, in the presence of 20 mol.% of CH_3OH in air. Fig. 7A reveals a major peak located at $g = 2.002$, characteristic of Fe^{III} in an octahedral environment, in agreement with the $Fe_2(MoO_4)_3$ crystal structure [45–47]. A minor peak, with less intensity, appears at $g = 4.17$, which is characteristic of Fe^{III} species in a tetrahedral environment and is assigned to surface defects. The intensity of the Fe^{III} signal decreased with analysis time in the presence of the reactants mixture (Fig. 7A). Quick reduction of Fe^{III} to Fe^{II} species is noticed when starting the treatment followed by a slower reduction process (Fig. 7B). In agreement with the XPS results, there is no evidence of any presence of Mo^{V} species. An experiment under drastic reducing conditions (20 mol.% of CH_3OH in Ar at 528 K) has also been performed with the aim at forcing total reduction of the catalyst. Only a decrease in the Fe^{III} quantity was observed with time on stream, whereas Mo centres remained in the Mo^{VI} state, indicating that the reduction of the catalyst is indeed exclusively owing to the reduction of iron species.

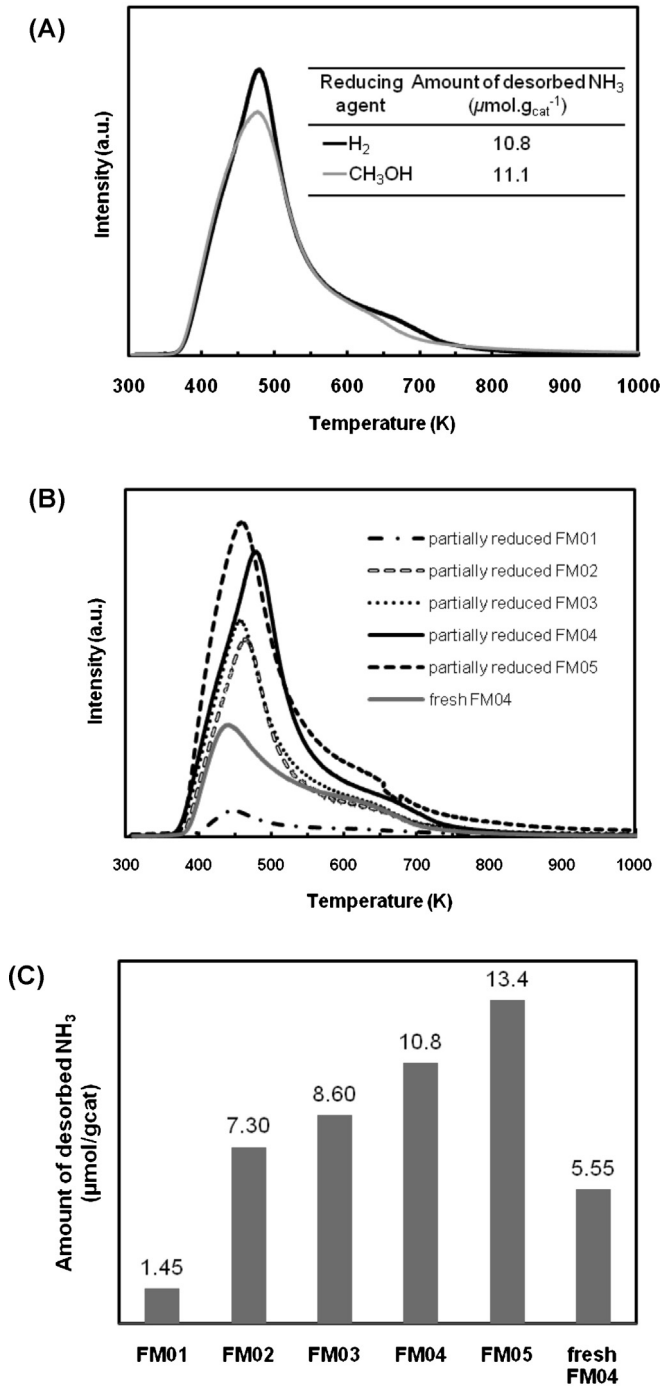

Fig. 8. (A) Experimental TPD of NH_3 curves for partially reduced FM04 sample using H2 (black line) and CH_3OH (grey line) as reducing agents; (B) experimental TPD of NH_3 curves for fresh and partially reduced by H_2 FeMo samples; (C) amount of desorbed NH_3.

3.3.4. Temperature-programmed desorption

The acidity of iron molybdate catalysts with different Mo/Fe ratios was examined by means of NH_3-TPD experiments. For experimental reasons, we chose to reduce the catalysts with H_2 instead of methanol. In order to be sure that the reduction by H_2 or CH_3OH leads to the same results, we first checked on one sample (*i.e.*, FM04) whether reduction with methanol and H_2 gives the same result or not. As a result, we obtained essentially the same behaviour (Fig. 8A) and concluded that we could indeed run relevant experiments after hydrogen pre-reduction, which is much easier while being representative of the effect observed after methanol pre-reduction. For the NH_3-TPD curves shown in Fig. 8B, all the peaks appeared in the low-temperature region, below 673 K, thus suggesting the presence of weak acid sites [48]. In comparison with the freshly calcined sample, the amount of NH_3 desorbed from the surface of FM04 catalyst partially pre-reduced with H_2 is significantly higher (*i.e.*, 5.55 μmol NH_3 g_{cat}^{-1} *vs.* 10.8 μmol NH_3 g_{cat}^{-1}). This implies that more acid sites have been formed after partial reduction. Furthermore, the newly formed acids sites upon reduction are stronger, according to a shift of the temperature of the peak from 440 to 480 K. During the reaction course, the catalyst is being continuously slightly reduced due to the presence of methanol, even if only a partial reduction is observed. The gradual increase in selectivity observed during the first reaction hours (*cf.* Section 3.2, Fig. 2B) can be ascribed to an increase in the surface acidity, which is relevant for DMM formation. In addition, the amount of desorbed NH_3 increases from 1.45 to 13.4 μmol NH_3 g_{cat}^{-1} with increasing the Mo/Fe ratio from 2.5 to 3.9 (Fig. 8C), which is proportional to the Mo content in the catalyst.

3.3.5. Active site for methanol oxidation to DMM

Both conversion and selectivity increases with time on stream under reaction conditions can then be explained taking into account the reducibility and acidity of the iron molybdate mixed oxide catalysts. The catalytic results on single oxides show that either Fe or Mo is able to activate methanol. Clearly, there is a synergistic effect when both elements are present together, possibly in strong interaction. With respect to surface analysis results (XPS), molybdenum is being in contact with methanol during reaction meanwhile the partial reduction is taking place intensively on iron. The surface and bulk ratios between molybdenum and iron, determined by XPS and ICP-MS, respectively, is higher than that of stoichiometric iron molybdate (Mo/Fe = 1.5). It is known from the literature that the enrichment of Mo helps preventing the formation of Fe-rich phases, which can favour the oxidation reactions, due to the loss of Mo with water [49–52]. Moreover, in the studied series, the best catalyst contains a relatively high proportion of MoO_3 (36 rel.%; *cf.* Section 3.1, Table 1), ensuring the synergistic correlation between MoO_3 and $Fe_2(MoO_4)_3$ in agreement with what is observed for the selective oxidation of methanol to formaldehyde [53–55]. MoO_3 can generate Lewis acidity associated with Mo coordinatively unsaturated sites (CUS) [56]. Pernicone proposed that the acidity of the Fe–Mo oxide catalyst is connected with Lewis acid sites. On such sites, methanol chemisorption can take place, and they have been described as anionic vacancies produced by dehydroxylation of the catalyst surface [35].

It is known since a long time that methanol dissociatively chemisorbs over MoO_3 at temperatures as low as 298 K. Adsorption is thought to occur on coordinatively unsaturated surface Mo species and results in the formation of a surface methoxy and a surface hydroxyl groups [57–60]. It has been proposed that the methoxy groups decompose to formaldehyde and that the protons released from the alcohol react with lattice oxygen to form H_2O [57,58]. For the selective oxidation of methanol to formaldehyde, methoxy decomposition is believed to be the rate-limiting step of the reaction, while the incorporation of lattice oxygen into the produced water has been demonstrated with ^{18}O isotopic labelling [60] and, therefore, the reaction obeys to a redox mechanism of the Mars–van Krevelen type [57,61,62].

Coordinatively unsaturated ferrous (CUF) sites can also exist, and have been proposed as active sites over Pt–Fe bicomponent catalysts for catalytic oxidation reactions [63,64]. According to the literature on the crystalline structure of $Fe_2(MoO_4)_3$, one can assume that, for iron–molybdenum mixed oxide catalysts, MoO_4 tetrahedrons are linked with FeO_6 octahedra *via* oxygen atoms [45–47]. The active site, therefore, involves anionic vacancies and

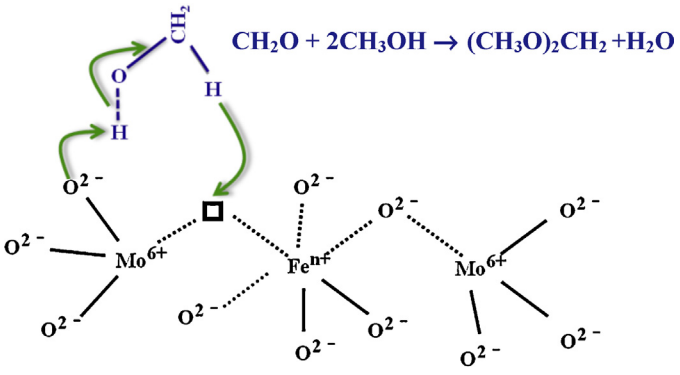

Scheme 2. Proposed active site for methanol transformation to DMM (Fe^{n+}: Fe^{3+} or Fe^{2+}, and □: anionic vacancy, number arbitrary).

O^{2-} species of the solid, as suggested by Pernicone [35], and our observed synergistic effect between Mo and Fe implies that such site intimately incorporates both Mo and Fe cations. Moreover, one can propose that the rate-determining step, related to the rupture of the C—H bond, could then correspond to a heterolytic rupture with the abstraction of a hydride species from methanol, which then would be located in the vacancy (Scheme 2).

It is possible that the activation of methanol takes place on an active site involving cooperation between Mo and Fe species, yielding adsorbed formaldehyde. NH_3-TPD experiments showed that the catalyst reduction leads to an increase in the acidity required to catalyze the sequential condensation/dehydration reaction between formaldehyde and two molecules of methanol to yield DMM. This acidity is provided by anionic vacancies, which are of the Lewis type [35,65], and the number/strength of the acid sites become larger upon the partial reduction of the catalyst with increasing numbers of vacancies. It is notable that the catalyst surface may contain both Lewis and Brønsted acid sites. The latter ones are generated in the presence of water formed during reaction, by Lewis sites hydration. As a matter of fact, this interchange between Lewis and Brønsted acids can also enhance/modify the surface acidity, which is required for acetalization reaction. As a specific feature of the FeMo catalysts, the formation of DMM is facilitated using high concentrations of methanol in the feed. Gaseous oxygen present in the reaction medium is not directly involved in the oxidation reaction, but is responsible for the surface reoxidation of Fe^{II} species in agreement with the Mars–van Krevelen mechanism [57,61,62] and/or react with speculated hydride species regenerating the active sites as described in Eqs. (a) and (b) [66].

$$H^- + \tfrac{1}{2}O_2 \rightarrow OH^- \quad \text{(a)}$$

$$2OH^- \rightarrow O^{2-} + \square + H_2O \quad \text{(b)}$$

However, further studies are still needed to propose a complete mechanism. As a matter of fact, all the methanol molecules can be adsorbed on the surface and specific active sites can lead directly to DMM. Hydrogen abstraction from methanol, and thus formation of hydrogen on the solid, can be linked to the reduction of Fe^{III} to Fe^{II}. Nonetheless, the reactivity between hydride species on the solid and oxygen in the gas phase should be very fast, and this phenomenon can explain the slow reduction of the catalyst and the good stability of the catalytic performances.

4. Conclusions

We report herein an efficient iron molybdate mixed oxide catalyst for the gas phase selective conversion of methanol to *1,1*-dimethoxymethane (DMM) using a methanol-rich reactants mixture. Catalysts with different Mo and Fe contents were synthesized by the coprecipitation technique before being calcined at 723 K in air. The highest DMM yield with a selectivity of 85% for 46% conversion was obtained at 528 K over the catalyst with a bulk Mo/Fe ratio of 3.4 (Fe/M_T = 0.228). This catalyst contained 64% of crystalline $Fe_2(MoO_4)_3$ and 36% of crystalline MoO_3, with a relatively high surface area compared to the other catalysts of the studied series. The good performance in terms of DMM production can be ascribed to the concomitant redox and acid properties present in the Fe–Mo–O catalytic system, which are relevant to undergo consecutive partial oxidation and condensation reactions. Surface composition and reducibility were investigated by LEIS and XPS. With respect to the LEIS results, the outermost surface layer of the fresh catalyst presented both Mo and Fe species with a Mo/Fe ratio of 3. From the XPS analysis results, we deduced that the direct synthesis of DMM from methanol using the feed highly concentrated in methanol involves adsorption of methanol on the sites where Mo and Fe atoms are connected. This leads to the partial reduction of some Fe from Fe^{III} to Fe^{II} on the catalyst surface. The same phenomenon was also characterized by the EPR experiments. These catalytic active sites were proposed as anionic vacancies – which can be generated by surface dehydroxylation and are identified as Lewis acid sites surrounded by Mo and Fe atoms. Acidity of the catalyst was determined by NH_3-TPD. The number of acid sites and their strength were increased by pre-reducing the catalyst with H_2. As the catalyst is being continuously reduced under the reducing atmosphere applied during the reaction, due to the presence of methanol, a significant increase in selectivity can be attributed to an increase in acidity, which is required in the acetalization reaction to form DMM, in addition to the redox properties. Owing to the reduction of the catalyst, the number of anionic vacancies became larger. This helped improving the catalytic conversion. Evidence was reported that gaseous oxygen is only responsible for reoxidizing the catalyst surface, especially Fe sites, suggesting that the studied reaction obeys the Mars–van Krevelen mechanism. At last, we observed a synergistic influence between Mo and Fe in the catalyst, particularly on methanol conversion. By advisedly optimizing the Fe–Mo–O catalyst formulation, an optimal DMM yield could be achieved, *i.e.*, the formulation with Mo/Fe ratio of 3.4 could reach the extrapolated yield value of 50% yield.

Alternatively for methanol oxidation to formaldehyde, this study demonstrates also the importance of the methanol partial pressure but mostly the importance of the average oxidation state on the selectivity. For the formation of DMM, catalyst formulations should be tuned to keep the balancing of oxidation states (*i.e.*, Fe^{III} and Fe^{II}) present during the course of reaction.

Acknowledgements

The research leading to these results has received funding from the European Union Seventh Framework Program (FP7/2007-2013) under grant agreement n° 241718 EuroBioRef. The authors would like to thank Mrs. Laurence Burylo and Mrs. Caroline Pirovano from UCCS for their technical help and fruitful discussions. The "Fonds Européen de Développement Régional (FEDER)", "CNRS", "Région Nord Pas-de-Calais" and "Ministère de l'Education Nationale de l'Enseignement Supérieur et de la Recherche" are also acknowledged for fundings of X-ray diffractometers and of XPS/LEIS/ToF-SIMS spectrometers.

References

[1] EP Pat. 1914293 (2008).
[2] WO Pat. 090294 (2008).
[3] J.C. Ball, C. Lapin, J. Buckingham, E. Frame, D. Yost, M. Gonzalez, E. Liney, M. Natarajan, J. Wallace, SAE Transaction Section 4 110 (2001) 2176–2181.
[4] M. Matti Maricq, R.E. Chase, D.H. Podsiadlik, W.O. Siegl, E.W. Kaiser, SAE Transaction Section 4 107 (1998) 1504–1509.

[5] Q. Sun, A. Auroux, J. Shen, Journal of Catalysis 244 (2006) 1–9.
[6] R. Chetty, K. Scott, Journal of Power Sources 173 (2007) 166–171.
[7] D. Devaux, H. Yano, H. Uchida, J.-L. Dubois, M. Watanabe, Electrochimica Acta 56 (2011) 1460–1465.
[8] F. Vigier, C. Coutanceau, J.M. Léger, J.L. Dubois, Journal of Power Sources 175 (2008) 82–90.
[9] G. Lambiotte, CH Pat. 688041 (1997).
[10] WO Pat. 018209 (1993); EP Pat. 704442 (1996); US Pat. 5959456 (1999); US Pat. 6160174 (2000); US Pat. 6160186 (2000); US Pat. 6166266 (2000); 2002; US Pat. 6437195 (2002); US Pat. 6379507 (2002).
[11] M. Fournier, A. Aouissi, C. Rocchiccioli-Deltcheff, Journal of the Chemical Society, Chemical Communications (1994) 307–308;
C. Rocchiccioli-Deltcheff, A. Aouissi, M.M. Bettahar, S. Launay, M. Fournier, Journal of Catalysis 164 (1996) 16–27;
C. Rocchiccioli-Deltcheff, A. Aouissi, S. Launay, M. Fournier, Journal of Molecular Catalysis A: Chemical 114 (1996) 331–342.
[12] H. Liu, E. Iglesia, The Journal of Physical Chemistry B 107 (2003) 10840–10847; H. Liu, E. Iglesia, Journal of Catalysis 223 (2004) 161–169.
[13] H. Liu, E. Iglesia, Journal of Physical Chemistry B 109 (2005) 2155–2163.
[14] T. Kotbagi, D.L. Nguyen, C. Lancelot, C. Lamonier, K.-A. Thavornprasert, Z. Wenli, M. Capron, L. Jalowiecki-Duhamel, S. Umbarkar, F. Dumeignil, ChemSusChem 5 (2012) 1467–1473.
[15] Y. Yuan, H. Liu, H. Imoto, T. Shido, Y. Iwasawa, Chemistry Letters (2000) 674–675;
Y. Yuan, H. Liu, H. Imoto, T. Shido, Y. Iwasawa, Journal of Catalysis 195 (2000) 51–61;
Y. Yuan, T. Shido, Y. Iwasawa, Chemical Communications (2000) 1421–1422;
Y. Yuan, Y. Iwasawa, Journal of Physical Chemistry B 106 (2002) 4441–4449;
Y. Yuan, K. Tsai, H. Liu, Y. Iwasawa, Topics in Catalysis 22 (2003) 9–15.
[16] A. Tougerti, S. Cristol, E. Berrier, V. Briois, C. La Fontaine, F. Villain, Y. Joly, Physical Review B 85 (2012) 1–8.
[17] X. Sécordel, A. Yoboué, S. Cristol, C. Lancelot, M. Capron, J.-F. Paul, E. Berrier, Journal of Solid State Chemistry 184 (2011) 2806–2811.
[18] O.A. Nikonoa, M. Capron, G. Fang, J. Faye, A.-S. Mamede, L. Jalowiecki-Duhamel, F. Dumeignil, G.A. Seisenbaeva, Journal of Catalysis 279 (2011) 310–318.
[19] Y. Fu, J. Shen, Chemical Communications (2007) 2172–2174.
[20] J. Liu, Y. Fu, Q. Sun, J. Shen, Microporous Mesoporous Materials 116 (2008) 614–621;
J. Liu, Q. Sun, Y. Fu, J. Shen, Journal of Colloid Interface Sciences 335 (2009) 216–221;
H. Zhao, S. Bennici, J. Shen, A. Auroux, Journal of Molecular Catalysis A: Chemistry 309 (2009) 28–34;
W. Li, Y. Sun, Catalysis Communications 11 (2010) 396–400;
H. Zhao, S. Bennici, J. Shen, A. Auroux, Journal of Thermal Analysis and Calorimetry 99 (2010) 843–847;
H. Guo, D. Li, D. Jiang, W. Li, Y. Sun, Catalysis Letters 135 (2010) 48–56;
H. Zhao, S. Bennici, J. Shen, A. Auroux, Journal of Catalysis 272 (2010) 176–189;
H. Zhao, S. Bennici, J. Cai, J. Shen, A. Auroux, Catalysis Today 152 (2010) 70–77.
[21] Q. Sun, Y. Fu, J. Liu, A. Auroux, J. Shen, Applied Catalysis A 334 (2008) 26–34.
[22] E. Tronconi, A.S. Elmi, N. Ferlazzo, P. Forzatti, G. Busca, P. Tittarelli, Industrial & Engineering Chemistry Research 26 (1987) 1269–1275.
[23] G. Deo, I.E. Wachs, Journal of Catalysis 146 (1994) 323–334.
[24] X. Lu, Z. Qin, M. Dong, H. Zhu, G. Wang, Y. Zhao, W. Fan, J. Wang, Fuel 90 (2011) 1335–1339.
[25] S. Chen, S. Wang, X. Ma, J. Gong, Chemical Communications 47 (2011) 9345–9347.
[26] H. Guo, D. Li, C. Chen, Z. Fan, Y. Sun, Chinese Journal of Catalysis 33 (2012) 813–818.
[27] H. Golinska-Mazwa, P. Decyk, M. Ziolek, Journal of Catalysis 284 (2011) 109–123.
[28] S. Royer, X. Sécordel, M. Brandhorst, F. Dumeignil, S. Cristol, C. Dujardin, M. Capron, E. Payen, J.-L. Dubois, Chemical Communications 7 (2008) 865–867.
[29] J.M. Tatibouët, J.E. Germain, Journal of Catalysis 72 (1981) 375;
J.-M. Tatibouët, Applied Catalysis A 148 (1997) 213–252;
J.-M. Tatibouët, H. Lauron-Pernot, Journal of Molecular Catalysis A: Chemistry 171 (2001) 205–216.
[30] J.-L. Dubois, M. Brandhorst, M. Capron, C. Dujardin, WO 2007/034264 (2007).
[31] J. Gornay, X. Sécordel, M. Capron, G. Tesquet, P. Fongarland, E. Payen, J.-L. Dubois, F. Dumeignil, Oil & Gas Science and Technology 65 (2010) 751–762.
[32] I.E. Wachs, US Pat. 6 875 724 (2005).
[33] J. Gornay, X. Sécordel, G. Tesquet, B. de Ménorval, S. Cristol, P. Forgarland, M. Capron, L. Duhamel, E. Payen, J.-L. Dubois, F. Dumeignil, Green Chemistry 12 (2010) 1722–1725.
[34] N. Pernicone, F. Lazzerin, G. Liberti, G. Lanzavecchia, Journal of Catalysis 14 (1969) 293–302.
[35] N. Pernicone, Journal of the Less-Common Metals 36 (1974) 289–297.
[36] H.H. Brongersma, T. Grehl, P.A. van Hal, N.C.W. Kuijpers, S.G.J. Mathijssen, E.R. Schofield, R.A.P. Smith, H.R.J. ter Veen, Vacuum 84 (2010) 1005–1007.
[37] N. Fairley, www.casaxps.com
[38] M. Brandhorst, S. Cristol, M. Capron, C. Dujardin, H. Vezin, G. Lebourdon, E. Payen, Catalysis Today 113 (2006) 34–39.
[39] D. Massiot, F. Fayon, M. Capron, I. King, S. Le Calvé, B. Alonso, J.-O. Durand, B. Bujoli, Z. Gan, G. Hoatson, Magnetic Resonance in Chemistry 40 (2002) 70–76.
[40] T. Yamashita, P. Hayes, Applied Surface Sciences 254 (2008) 2441–2449;
M.C. Biesinger, B.P. Payne, A.P. Grosvenor, L.W.M. Lau, A.R. Gerson, R.St.C. Smart, Applied Surface Sciences 257 (2011) 2717–2730.
[41] A.P. Grosvenor, B.A. Kobe, M.C. Biesinger, N.S. McIntyre, Surface and Interface Analysis 36 (2004) 1564–1574.
[42] Y.V. Plyuto, I.V. Babich, I.V. Plyuto, A.D. Van Langeveld, J.A. Moulijn, Applied Surface Science 119 (1997) 11–18.
[43] L. Briand, O. Tkachenko, M. Guraya, I.E. Wachs, W. Grünert, Surface and Interface Analysis 36 (2004) 238–245.
[44] X. Huang, J. Liu, J. Chen, Y. Xu, W. Shen, Catalysis Letters 108 (2006) 79–86.
[45] M.H. Rapposch, J.B. Anderson, E. Kostiner, Inorganic Chemistry 19 (1980) 3531–3539.
[46] H.Y. Chen, Materials Research Bulletin 14 (1979) 1583–1590.
[47] G. Fagherazzi, N. Pernicone, Journal of Catalysis 16 (1970) 321–325.
[48] F. Lonyl, J. Valyon, Microporous Mesoporous Materials 47 (2001) 293–301;
M. Sawa, M. Niwa, Y. Murakami, Zeolites 10 (1990) 532–538.
[49] A.P.V. Soares, M. Farinha Portela, A. Kiennemann, L. Hilaire, J.M.M. Millet, Applied Catalysis A-General 206 (2001) 221–229.
[50] A.P.V. Soares, M. Farinha Portela, A. Kiennemann, L. Hilaire, Chemical Engineering Science 58 (2003) 1315–1322.
[51] G. Shi, T. Franzke, M.D. Sánchez, W. Xia, F. Weis, M. Seipenbusch, G. Kasper, M. Muhler, ChemCatChem 4 (2012) 760–765.
[52] M.P. House, A.F. Carley, R. Echeverria-Valda, M. Bowker, Journal of Physical Chemistry C 112 (2008) 4333–4341.
[53] E. Soderhjelm, M. House, N. Cruise, J. Holmberg, M. Bowker, J.-O. Bovin, A. Anderson, Topics in Catalysis 50 (2008) 145–155.
[54] I.E. Wachs, Journal of Catalysis 275 (2010) 84–98.
[55] G. Jin, W. Weng, Z. Lin, N.F. Dummer, S.H. Taylor, C.J. Kiely, J.K. Bartley, G.J. Hutchings, Journal of Catalysis (2012), http://dx.doi.org/10.1016/j.jcat.2012.09.001.
[56] I. Matsuura, S. Mizuno, H. Hashiba, Polyhedron 5 (1986) 111–117.
[57] W.E. Farneth, F. Ohuchi, R.H. Staley, U. Chowdhry, A.W. Sleight, Journal of Physical Chemistry 89 (1985) 2493–2497.
[58] W.E. Farneth, R.H. Staley, A.W. Sleight, Journal of American Ceramic Society 108 (1986) 2327–2332.
[59] J.S. Chung, R. Miranda, C.O. Bennett, Journal of Catalysis 114 (1988) 398–410.
[60] C.J. Machiels, A.W. Sleight, Journal of Catalysis 76 (1982) 238–239.
[61] P. Mars, D.W. van Krevelen, Chemical Engineering Science 3 (1954) 41–59.
[62] G. Busca, Catalysis Today 27 (1996) 457–496.
[63] Q. Fu, W.-X. Li, Y. Yao, H. Liu, H.-Y. Su, D. Ma, X.-K. Gu, L. Chen, Z. Wang, H. Zhang, B. Wang, X. Bao, Science 328 (2010) 1141–1144.
[64] H. Xu, Q. Fu, Y. Yao, X. Bao, Energy and Environmental Sciences 5 (2012) 6313–6320.
[65] M. Gotić, G. Koščec, S. Musić, Journal of Molecular Structure 924–926 (2009) 347–354.
[66] C. Pirez, M. Capron, H. Jobic, F. Dumeignil, L. Jalowiecki-Duhamel, Angewandte Chemie International Edition 50 (2011) 10193–10197.